

Wireless microwave-to-optical conversion via programmable metasurface without DC supply

Received: 17 July 2024

Accepted: 2 January 2025

Published online: 09 January 2025



Xin Ge Zhang^{1,7}, Ya Lun Sun^{1,7}, Bingcheng Zhu^{2,7}, Han Wei Tian¹, Bo Yuan Wang¹,
Zaichen Zhang^{2,3,4} ✉, Cheng-Wei Qiu⁵ ✉, Tie Jun Cui^{1,6} ✉ &
Wei Xiang Jiang^{1,3,4} ✉

Microwave-optical interaction and its effective utilization are vital technologies at the frontier of classical and quantum sciences for communication, sensing, and imaging. Typically, state-of-the-art microwave-to-optical converters are realized by fiber and circuit approaches with multiple processing steps, and external powers are necessary, which leads to many limitations. Here, we propose a programmable metasurface that can achieve direct and high-speed free-space microwave-to-laser conversion. Moreover, it supports reverse conversion, achieving bidirectional operations. The programmable metasurface converter is realized by integrating subwavelength microwave resonant structures, MS junction and photoelectric PN junction components together, without connecting any direct-current supplies to provide driving bias. We further demonstrate the enormous potentials of the metasurface converter in cross-media links and develop a full-duplex air-water wireless communication system. Experimental results show that the bidirectional real-time data transmissions and exchanges are established through the air-water boundary. This work represents a decisive step towards microwave-optical interconversion on wireless and battery-free interfaces.

Conversions of energy and information between microwave and optical domains are essential in numerous fields, from telecommunication to emerging quantum technologies^{1–3}. The microwave-optical interaction platform can not only connect systems in the electrical and optical domains, but also leverage fully the advantages of microwaves and light waves in different propagation media to achieve seamless cross-media transmission, which is a valuable solution in next generation fully-connected information systems and networks^{4–10}. However, effective microwave-optical interactions present an immense challenge due to the natural incompatibility of energies caused by significant frequency scale mismatch of $>10^4$. In recent years, much effort has been

focused on this conversion task using fiber technology, plasmonic cavities, nonlinear materials, nanomechanical coupling, Rydberg excitons, intermediary-assisted approach, and so on^{11–18}. However, many demonstrated microwave-to-optical conversion schemes are realized based on fiber and circuit technologies, and external power suppliers are required to perform multiple intermediate processes, which increases the cost, power consumption, and system complexity, as well as restricting the free-space wireless applications. Moreover, these conversion devices are hard to further develop for achieving reverse process from optical to microwave, resulting in many limitations.

¹State Key Laboratory of Millimeter Waves, School of Information Science and Engineering, Southeast University, Nanjing, China. ²National Mobile Communications Research Laboratory, School of Information Science and Engineering, Southeast University, Nanjing, China. ³Frontiers Science Center for Mobile Information Communication and Security, Southeast University, Nanjing, China. ⁴Purple Mountain Laboratories, Nanjing, China. ⁵Department of Electrical and Computer Engineering, National University of Singapore, Singapore, Singapore. ⁶Suzhou Laboratory, Suzhou, China. ⁷These authors contributed equally: Xin Ge Zhang, Ya Lun Sun, Bingcheng Zhu. ✉e-mail: zc Zhang@seu.edu.cn; chengwei.qiu@nus.edu.sg; tjcu@seu.edu.cn; wxiang81@seu.edu.cn

In sharp contrast to the circuit-enabled solutions, metasurface, regarded as two-dimensional metamaterial, offers a new paradigm for manipulating free-space electromagnetic (EM) waves^{19–23}. Through special structural design and material composition, strong and controllable light–matter interactions can be well achieved on metasurface, providing unprecedented opportunities for spatial EM control^{24–28}, time-domain harmonic tailoring^{29–31}, and spatiotemporal modulation^{32–34}. Although metasurfaces have shown extraordinary potential across a wide spectrum ranging from microwave to terahertz and optics, high-speed intercoupling of waves with huge wavelength differences at single metasurface still remains elusive. Recently, light-controlled microwave metasurfaces have been realized, on which the microwave phase can be manipulated by illuminated light intensity^{35,36}. However, they can only achieve the unidirectional control from light to microwave at low speed. To enhance the speed, we previously reported the light-controlled time-domain metasurface with high-speed signal conversion³⁷, however, it also operates at light-to-microwave mode and needs an external power supply. How to achieve free-space microwave-to-optical conversion and even bidirectional operations on one metasurface is a key technology for developing full-duplex data transmission with enhanced efficiency and capacity; wireless and battery-free operation can release a lot of restrictions, but both remain considerably challenging.

Here, we report a programmable metasurface capable of direct and wireless microwave-to-optical conversion at physical layer, without using multiple separated devices and connecting any direct-current (DC) power supplies. Such a metasurface relies on the proposed hybrid integration of double-sided microwave resonant structures and two different types of semiconductor components based on rectifying effect and photo-capacitance effect, respectively. Therefore, it also supports reverse conversion from optical to microwave in free

space. Based on the metasurface, we design and realize a minimalist architecture of bidirectional cross-media wireless communications by combining microwaves and underwater lasers, and construct a system prototype by further developing the microwave and laser transceivers. In the hybrid system, two independent and simultaneous data transmission links of microwave-to-laser (from air to underwater) and laser-to-microwave (from underwater to air) are verified successfully, showing full-duplex and real-time communication capabilities. The bidirectional signal conversion is implemented fully on an ultrathin and wireless platform, offering great benefits in terms of cost, volume, integration, and deployment.

Results

Microwave-optical conversion empowered by metasurface

Figure 1a schematically illustrates the programmable metasurface and its attractive application in cross-media wireless communication to connect the sky and ocean. Signal conversion between microwave and optical domain is a fundamental function for this communication scenario using two different carriers. We first compare the existing techniques with our exciting metasurface-empowered approach. Traditionally, microwave-to-optical conversion relies on common microwave photonics techniques. In this scheme, the microwave signal (through transmission line) and optical carrier (through fiber) need to be input simultaneously, and then based on electro-optic modulation effect, the microwave data are mapped onto the output optical signal (Fig. 1b). Therefore, the entire process is wired and usually involves multiple processes including coupling, modulation, or even amplifying, resulting in power consuming and system complexity.

Our programmable metasurface provides distinctly different routes to implement free-space microwave-to-optical conversion, as shown in Fig. 1c. The input microwave signal can be converted directly

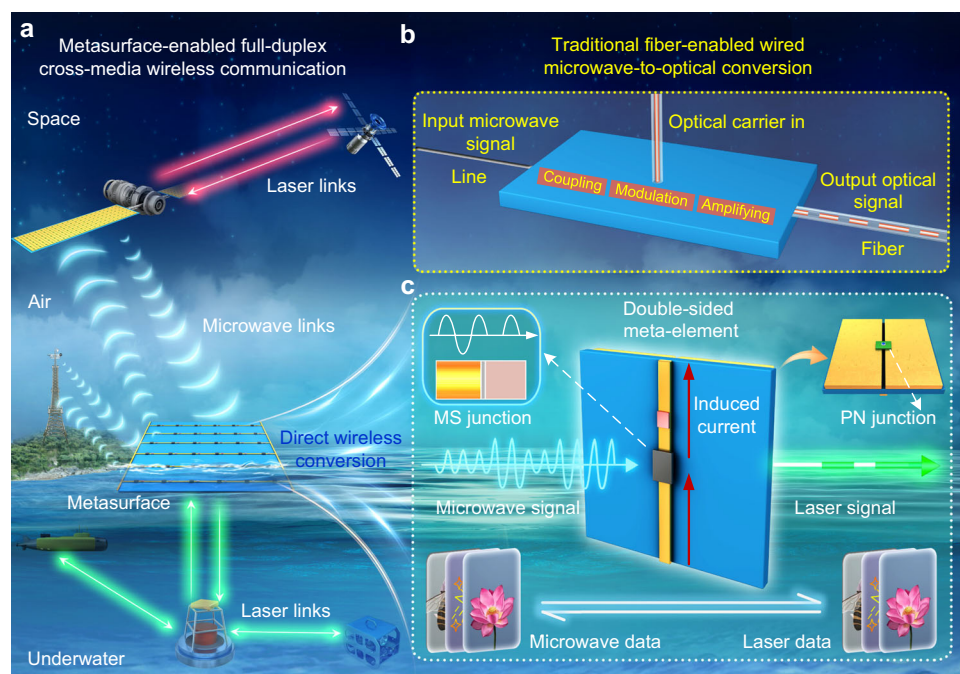


Fig. 1 | Existing wired scheme versus our metasurface-empowered wireless approach for microwave-optical conversion. **a** Schematic of the metasurface converter and its attractive application in full-duplex air–water cross-media wireless communications for establishing a seamless satellite–air–ground–ocean network. **b** Traditional microwave-to-optical conversion based on microwave photonics techniques, where the microwave signal and optical carrier need to be input simultaneously, and then the microwave data are mapped onto the output optical signal using electro-optic modulation. **c** Direct free-space microwave-to-optical

conversion using metasurface, which is realized by integrating MS junction and photoelectric PN junction components into meta-elements with double-sided microwave resonant structures. With this hybrid design, the input microwave signal can be converted directly into laser signal, without additional optical carrier feeding, wired power supplies, and separation processes. Moreover, the reverse conversion from laser to microwave can be also realized on one platform, achieving bidirectional operation.

into laser signal, without additional optical carrier feeding and wired DC supply, offering significant advantages of wireless conversion, simple process, and high flexibility. The metasurface contains many identical meta-elements, each of which is realized by integrating metal–semiconductor (MS) junction with absorbing-rectifying capability into the microwave resonant structure patched on monolayer substrate. When microwaves propagate onto the metasurface, the energy will be absorbed and then generate induced current, which will be further rectified into DC directly by the MS junction component (such as Schottky diode) to drive the integrated laser diode emitting. Therefore, the luminous intensity of the laser diode is related to the power level of incident microwave, achieving the wireless microwave-to-laser conversion.

Moreover, the metasurface platform provides a great deal of freedom for functional integration due to flexible design of artificial structures. Therefore, we further integrate the PN junction component (such as photodiode) into the backside of the ultrathin metasurface. In this case, as the laser illuminates the metasurface, the PN junction component will sense different intensities and generate capacitance changes, which in turn tunes the reflected amplitudes of incident microwave (see Supplementary Note 1 for more details on microwave incidence). Then, the reflected microwaves will carry the intensity information of incident laser, achieving the laser-to-microwave conversion. Therefore, based on different mechanisms, bidirectional and simultaneous conversions between microwave and laser can be realized directly on a single metasurface, without requirement for multiple separation devices to collaborate and complex signal-layer operations. Importantly, even if there is no power supply connection, the switching speed of the metasurface reaches the level of hundreds kHz. With these capabilities, the intensity-modulated microwave and optical signals can be converted to each other in real time, realizing the information modulations and full-duplex data transmissions.

The metasurface converter offers a data bridge linking the microwave and optical signals for cross-media wireless communications. The data transmission across the air–water interface is a solid foundation of the sixth-generation (6G) communication envisioned to achieve seamless global full coverage by integrating space–air–underwater networks, but faces significant challenges^{9,10}. A fundamental and critical one is that the air–water interface is a natural barrier to light and microwave alone. For example, in general, microwaves can propagate well in the air, while optical waves are highly potential candidates in the water, however, there will be great losses across the air–water boundary for both types of waves due to different properties of two media. As a result, it is difficult to communicate with multiple devices working in different media using single-form carrier signal, especially for long-distance case. To realize cross-media communication, appropriate carriers should be adopted to leverage their respective advantages in different transmission media. Our realized wireless metasurface provides an attractive solution for this purpose, as shown in Fig. 1a. The data collected by underwater equipment is transmitted through green laser links, and after modulating by metasurface, the converted microwave signals can be used to communicate with shore or even further converted into red laser signals by metasurface assembled on satellite to achieve direct inter-satellite interconnection. Similarly, the data can also be transmitted from air to underwater through the microwave-to-laser wireless link, establishing a seamless satellite–air–ground–ocean network.

Next, to show clearly the significant advantages of metasurface-enabled cross-media wireless communications, we will make some comparisons with current approaches. Communication across the air–water interface is an open research problem and many different avenues have been proposed, which can be divided into two categories^{9,10,38–43}. The first techniques rely on a typical relay scheme, in which hybrid systems, such as acoustic-microwave, microwave-optical conversion relays, need to be developed and equipped on buoys,

ships, or autonomous underwater vehicles^{38,39}. In this case, underwater devices transmit data via underwater acoustic or optical communication to surface relay nodes that then use microwave signals to transmit these data over the air. With the relay systems, acoustic, radio frequency and optical technologies can be integrated synergistically to achieve air–water cross-media communication. However, they also bear some limitations. On one hand, the current relay conversion devices require power suppliers, which is very inconvenient for scalable, long-term, in situ working, especially in extreme environments such as the ocean and space⁴⁴. On the other hand, these relay systems typically require intermediate processing at signal layer, resulting in complicated hardware and high overhead. The second is non-relay scheme, where the photoacoustic⁴⁰, magnetic induction⁴¹, and acoustic-to-radar^{42,43} technologies have been investigated to achieve direct air–water cross-media communication, offering several advantages of convenience and flexibility. However, the realized cross-media communication is unidirectional, i.e., the data can only transmit from underwater to air or from air to underwater. In addition, the communication rate is low. It is noted that unlike these traditional schemes, our realized approach achieves microwave-optical bidirectional conversion in a wireless mode, and importantly the entire conversion process is completed fully on an integrated ultrathin metasurface.

Design and realization of metasurface converter

To implement the metasurface converter, two key conditions must be met simultaneously. One is that the single metasurface must be able to interact with both microwave and optical fields simultaneously and then generate the microwave-optical intercoupling. The other is that the above process should be realized well in a DC-supply-free manner. We here adopt heterogeneous strategy and some key techniques including polarization multiplexing, EM resonance, photoelectric conversion, and integrated absorption-rectification to achieve the goal. The designed metasurface element is presented in Fig. 2a. The metal pattern on the top layer is a designed microwave Resonant Structure 1, in which a Schottky diode with the MS junction is integrated between two metal lines. When the microwave propagates into the meta-element, Resonant Structure 1 will absorb the microwave energy and then further rectify it to drive the integrated laser diode emitting, achieving the up-conversion from microwave to laser. Importantly, unlike the separate combination of absorber and rectifier, the loaded Schottky diode acts as a tuning component to achieve an integration of absorption and rectification. To further realize the laser-to-microwave down-conversion using the single meta-element, we design the microwave Resonant Structure 2 integrated with a photodiode. When the laser illuminates meta-element, the photodiode will absorb energy and generates the capacitance changes based on the photo-capacitance effect, which in turn affects the microwave resonance characteristics of the meta-element. In this case, the reflected microwave amplitude is related to the incident laser intensity. It should be noted that the entire meta-element has only one dielectric layer and two different metal resonant patterns are etched on the both sides, resulting in a very thin profile with $-0.027\lambda_0$ (λ_0 is the wavelength in free space) at 4.00 GHz. See “Methods” for more detailed discussion on meta-element design.

In sharp contrast to traditional diode-based metasurfaces that require power supplies to provide bias voltage for loaded diodes, our microwave-optical interconversion metasurface does not need to be connected to any DC supplies. That is to say, it can operate in a wireless and battery-free mode. Under the microwave incidence, Resonant Structure 1 will induce a surface current (Supplementary Fig. 3) and then generates a potential across the cathode and anode of the Schottky diode. As the incident microwave power increases, the generated potential difference will be greater than the threshold voltage of the Schottky diode, and it will be driven on⁴⁵. We note that under the microwave incidence, the Schottky diode experiences both forward

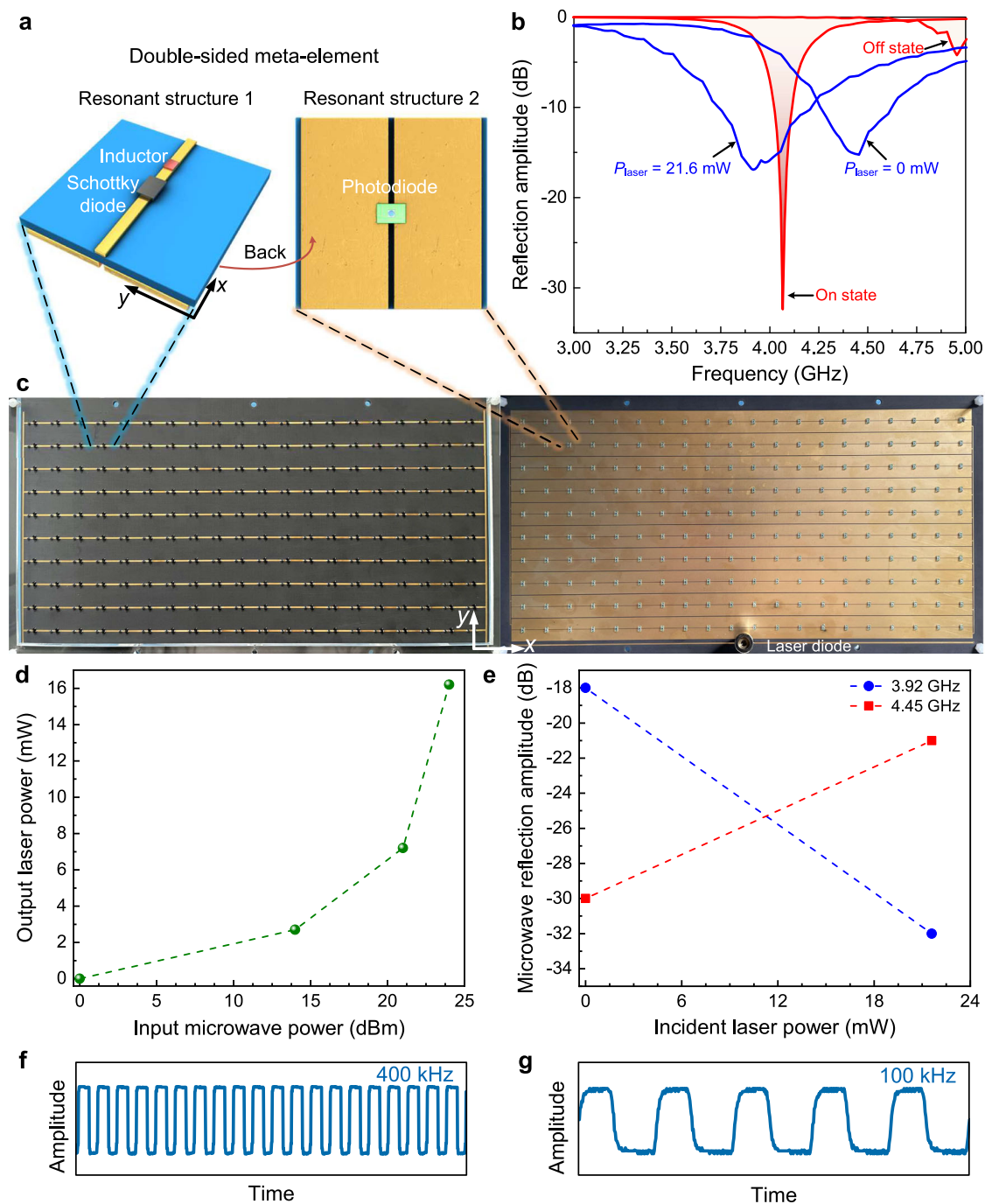


Fig. 2 | Metasurface and its microwave-laser interconversion performance. **a** Designed meta-element with double-sided microwave resonant structures, in which the Schottky diode and photodiode are integrated, respectively. **b** Simulated microwave reflection amplitudes of the meta-element under different conditions. **c** Photographs of Resonant Structures 1 (left) and Resonant Structures 2 (right) of the

metasurface sample. **d** Measured output green laser powers under different input microwave powers. **e** Measured microwave reflection amplitudes under different green laser illuminating powers. Measured switching speed of the Schottky-diode-based up-conversion metasurface (**f**) and the photodiode-based down-conversion metasurface (**g**).

and reverse biases instantaneously as the microwave signal cycles. That is to say, the Schottky diode conducts during the positive cycle of microwave signal and does not conduct during the negative cycle of microwave signal. For the photodiode, it can be used as an optically-controlled capacitor for tuning microwave resonance¹⁸, due to the light-induced space-charge region change. Remarkably, these two mechanisms do not require any external biases, and in essence, there are the microwave signal and laser signal themselves to drive Schottky diode and photodiode. In addition, to achieve low-crosstalk bidirectional conversion based on one meta-element, we adopt a polarization-

frequency joint isolation scheme. Specifically, the metal gaps in Resonant Structures 1 and 2 are orthogonal, so that they respond to orthogonally-polarized microwaves, and the resonant frequencies of these two structures are different.

To help further understand and evaluate the microwave-optical interconversion performance, we next investigate the resonant results of the meta-element. Here, we adopt the Schottky diode (HSMS-2860, from Avago) and photodiode (S13773, from Hamamatsu) to implement the meta-element according to our careful selection (see Supplementary Note 2 for more discussion on diode

selection and testing). Figure 2b shows the simulated reflection amplitude curves of the meta-element versus the frequency under different conditions. We observe clearly that when incident x-polarized microwave drives the Schottky diode in the on state, the meta-element produces a sharp resonance at around 4.00 GHz, indicating that the microwave energy is well absorbed. The absorbed microwave energy can be further rectified by the Schottky diode for driving the integrated laser diode emitting, thus achieving the up-conversion from microwave to laser. It is evident that under the y-polarized incidence, the meta-element produces a resonant response, and the resonant frequency shifts from 4.45 to 3.92 GHz as the incident laser power increases from 0 to 21.6 mW. In this case, two reflection amplitude differences of about 10 and 14 dB can be achieved at these two resonant frequencies, respectively. Therefore, the laser-to-microwave down-conversion can be well achieved. See Supplementary Note 3 for more details on meta-element simulation. We remark that when the x- or y-polarized waves propagate onto the meta-element, changing the state of the diode in the cross-polarization direction has no effect on the resonance response, as shown in Supplementary Fig. 6. In addition, the meta-element is operated at different microwave resonant frequencies for bidirectional conversions. Therefore, based on the polarization-frequency joint isolation, the realized meta-element can work well in a full-duplex mode.

Besides the implementation of meta-elements, we also design carefully their connections to achieve efficient microwave-laser inter-conversion. As a demonstration, we design a metasurface composed of 20×10 meta-elements and the corresponding fabricated sample is shown in Fig. 2c. The left part shows a photo of Resonant Structures 1 of the metasurface, where these 20 resonant structures in x-direction are connected in series and then are connected in parallel along the y direction. In this case, the collected power from all meta-elements can be combined to feed into the laser diode. The right photo presents Resonant Structure 2 of the metasurface, in which all the photodiodes are connected in parallel. In such a case, if one photodiode is illuminated and activated, the photogenerated potential difference will drive all other photodiodes to change their capacitances. Therefore, only a small laser beam is required to drive the metasurface to work, rather than a large spot to cover the entire metasurface, which reduces greatly the need for one-by-one alignment and the difficulty of light source design. In addition, to improve the switching speed, a resistor with an appropriate resistance value is connected in parallel to the photodiodes, providing a discharge circuit for photocarriers. As discussed later, the charge-discharge loop is crucial to improve the response speed of the photodiode. See “Methods” for more details on array design and sample fabrication.

To verify the microwave-to-laser conversion performance, we measure the output laser powers of the metasurface sample under different input microwave powers (see “Methods” for more details on experimental setup), and the measured results are presented in Fig. 2d. Here, the input microwave power refers to the microwave power fed into the transmitting horn antenna. It is obvious that the integrated green laser diode can indeed be well excited by the x-polarized microwave at 4.06 GHz. When the input microwave power reaches 14 dBm (25 mW), the laser diode is lit and the output laser power is 2.7 mW. Thus, the microwave-to-laser conversion efficiency is calculated as 10.8%. When the input microwave power is increased to 24 dBm (250 mW), the output laser power reaches 16.2 mW, and then the conversion efficiency is 6.48%. The difference in conversion efficiency is due to the fact that Schottky diode and laser diode are intensity-dependent nonlinear components. In our design, to reduce power consumption, we have chosen to use a low-power laser diode, and its own electro-optical conversion efficiency is low. Therefore, to improve the microwave-to-laser conversion efficiency, an effective approach is to use light-emitting diodes with higher electro-optical

efficiency. In addition, full-wave rectification scheme could be adopted to increase the rectification efficiency⁴⁶, however, it requires more Schottky diodes compared with current half-wave rectification.

We also test the microwave reflection amplitudes of the sample under different laser illumination intensities, as shown in Fig. 2e. It is clear that when the illuminated laser powers are changed between 0 and 21.6 mW, the sample can exhibit significantly different reflection amplitudes under y-polarized microwave incidences, and the differences reach 14 and 9 dB at 3.92 and 4.45 GHz, respectively. The measured results agree well with the simulated ones, which validates the efficient laser-to-microwave down-conversion. Moreover, based on the parallel design, each photodiode can be illuminated independently to generate the desired microwave reflection. We have measured the microwave reflection amplitudes of the metasurface at 4.45 GHz when photodiodes at different positions were illuminated, and the normalized results are shown in Supplementary Fig. 10. It is clear that when photodiodes at other positions are illuminated, the metasurface can generate the same reflection amplitude differences. In addition to illuminating one photodiode, the metasurface can also work well when the both photodiodes are illuminated simultaneously. Therefore, we can use a small laser beam to illuminate precisely and modulate the metasurface, and multiple photodiodes provide the possibility for spatial diversity receiving. Unlike the microwave-to-laser conversion which needs strong microwave power to drive the laser diode, we note that the required microwave power for the optical-to-microwave conversion is low. In the experiment, the power of the microwave source is 1 mW. Because we detect the power changes in the reflected microwave signals, a significant difference in the reflected energy is required, rather than a high incident power.

It is worth noting that the high-speed response is highly desirable for time-domain signal conversion, and we further estimate the switching speed of the metasurface sample by observing the distortion of the output waveform under corresponding square-wave modulation. The tested switching frequencies of the Schottky-diode-based up-conversion metasurface and the photodiode-based down-conversion metasurface are illustrated in Fig. 2f, g, respectively. We observe clearly that for up-conversion metasurface when the switching frequency reaches 400 kHz, the output waveform can still maintain a good square wave due to the ultrafast Schottky diode with MS junction. For down-conversion metasurface, the switching frequency of the metasurface is about 100 kHz. The reason is that the large junction capacitance of the photodiode leads to long charge-discharge time. Considering this factor, to improve the response speed, we have used a parallel resistor to provide a charge-discharge current loop for the photodiodes. As a comparison, we have also measured the down-conversion switching frequency of the metasurface sample without the resistor and it is only about 200 Hz, which proves that our method has increased switching speed by ~500 times. We remark that such the switching frequencies of the metasurface are achieved in a DC-supply-free case.

Full-duplex cross-media wireless communications

The programmable metasurface shows excellent capability to implement bidirectional conversion between microwave and laser signals and hence can serve as an ideal platform for full-duplex microwave-laser hybrid wireless communication. As shown in Fig. 2d, e, on-off laser intensities correspond to two different microwave intensities, suggesting that the on-off keying (OOK) laser signal and binary amplitude shift keying (BASK) microwave signal can be adopted to realize modulation and transmission of digital symbols “1” and “0”. The schematic of the proposed cross-media hybrid wireless communication is illustrated in Fig. 3a. Specifically, the metasurface-enabled hybrid wireless links are capable of emitting information through microwave and receiving it via laser, while also transmitting information via laser and receiving it via microwave. For microwave-to-laser

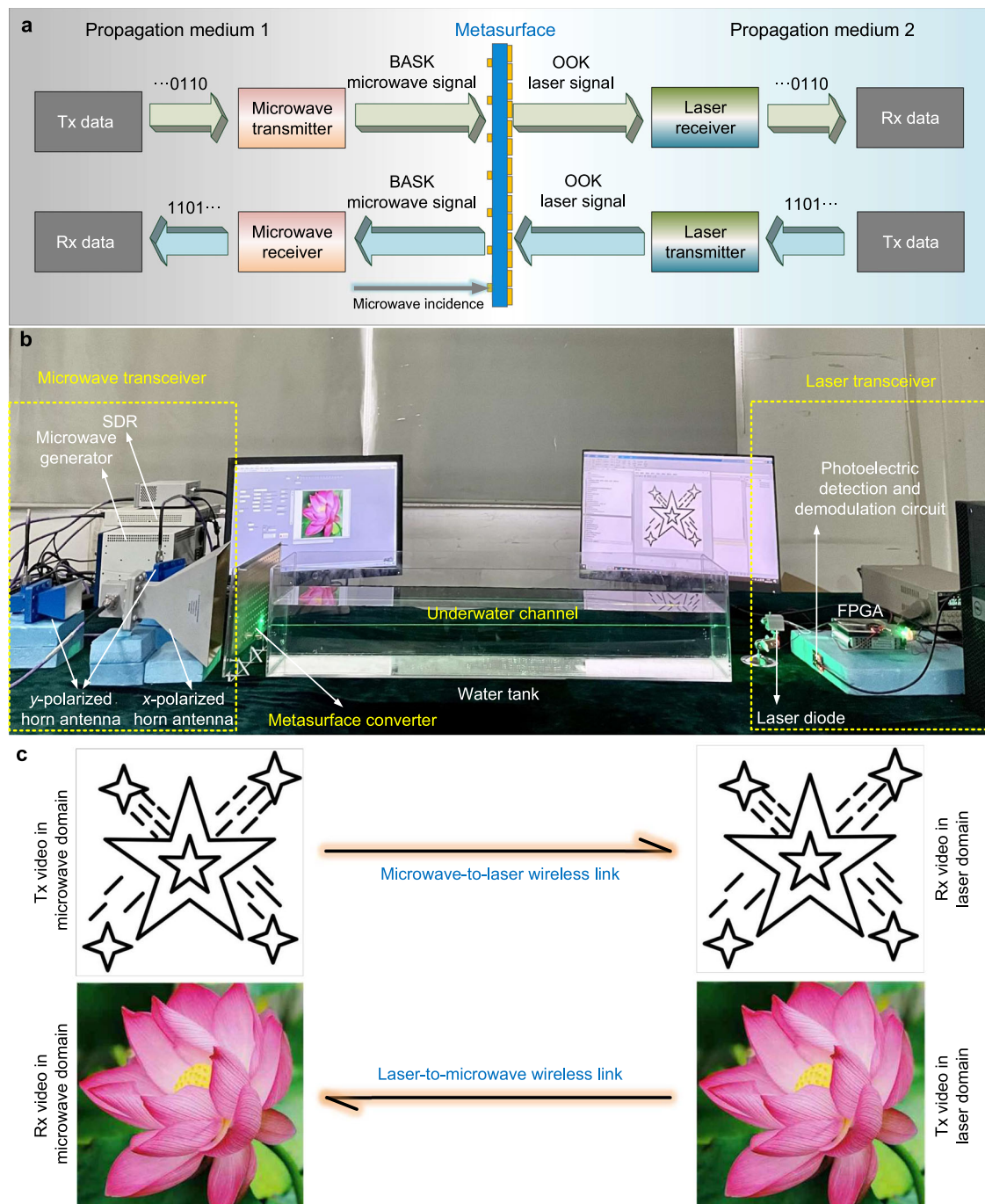


Fig. 3 | Experiments of the metasurface-enabled full-duplex air–water cross-media wireless communication system. **a** Schematic of the air–water cross-media wireless communication system with the hybrid air microwave link and underwater laser link. **b** Photograph of the constructed system prototype. The system contains a microwave transceiver, a metasurface converter, and a laser transceiver, in which

the water tank is placed between the latter two for providing the underwater channel. **c** Experimental results demonstrate that two different videos can be transmitted independently and simultaneously cross bidirectional air–water interfaces through the microwave-to-laser link and laser-to-microwave link, respectively.

wireless transmission link, real-time information transmission and reception are divided into three steps. Firstly, the transmitting data (Tx data) is modulated onto the BASK microwave signal through a designed microwave transmitter. After mapping by the metasurface, the transmitted BASK microwave signal is converted into an OOK laser signal. Finally, the OOK laser signal is received and demodulated by a designed laser receiver to restore the receiving data (Rx data). For down-conversion transmission process, the data is first modulated by a laser transmitter to generate an OOK laser signal, which is further converted into a reflected BASK microwave signal by the metasurface.

Finally, it is captured and demodulated into original data by the designed microwave receiver. It is worth highlighting that this bidirectional real-time information transmission process is full-duplex and minimalist, and is based on the metasurface without needing power supplies and mixers.

To validate the above scheme, we construct a metasurface-enabled full-duplex microwave-laser hybrid wireless communication system across the air–water interface, as shown in Fig. 3b. In this communication system, besides metasurface converter, the design and realization of microwave transceiver and laser transceiver are also

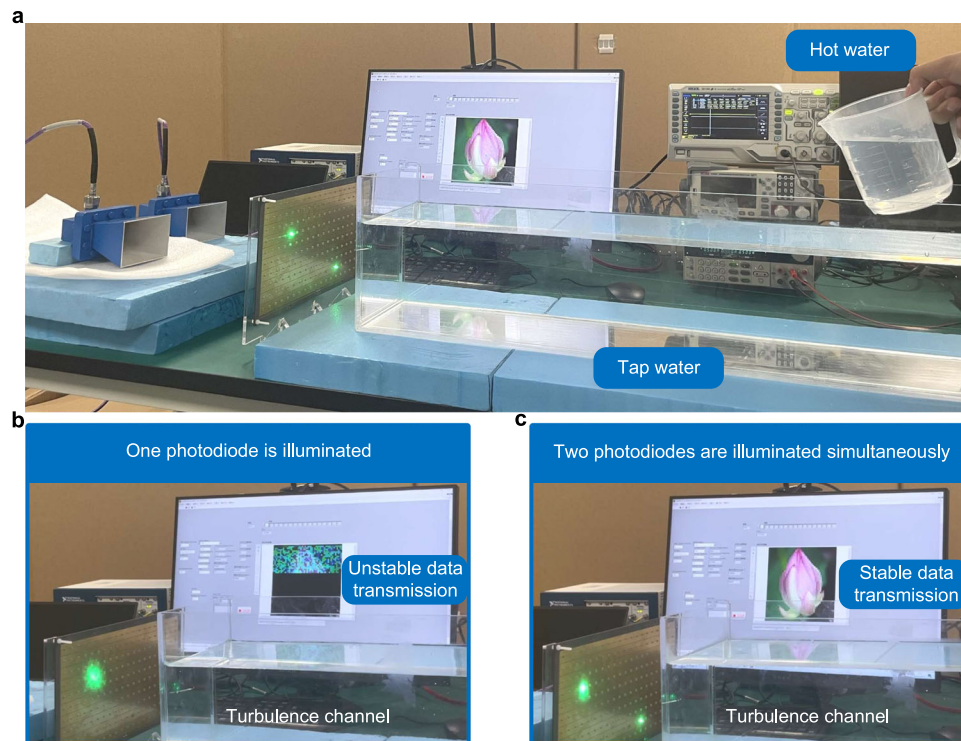


Fig. 4 | Experiments of the wireless transmission across underwater turbulence channel. **a** Photograph of the experimental setup, in which tap water is first injected into the water tank, and then hot water is injected into it from the top to bottom to generate temperature-induced turbulence. **b** For the case that one photodiode is illuminated, strong turbulence will cause the laser beam diffusion

and drift, which will reduce the transmission quality of the link. **c** The link can provide relatively stable data transmission when two photodiodes are illuminated simultaneously, even though one laser beam is in outage, the other can still ensure reliable operation.

important. The microwave transceiver is used to provide microwave signal for microwave-to-laser conversion and to receive the reflected microwave in laser-to-microwave link. The laser transceiver is adopted to provide laser signal for laser-to-microwave conversion and to receive generated laser in microwave-to-laser link. To verify this two-way data transmission cross the air-water media, a transparent water tank with a length of 1.0 m filled with tap water was adopted to simulate the underwater channel. The water tank is placed between the laser transceiver and the back side of the metasurface sample. In this case, the underwater laser communication links between the metasurface and laser transceiver can be established. At the front side of metasurface, the microwave transceiver was used to realize microwave communication links. Therefore, the bidirectional air-water cross-media wireless links can be performed based on the communication system. See “Methods” for more details on the system prototype.

To show the bidirectional and full-duplex air-water cross-media communication capability of our constructed microwave-laser hybrid wireless system, as an example, we demonstrate a real-time video transmission in the experiment, as shown in Fig. 3c. For microwave-to-laser transmission link across the air-to-water interface, the video (star twinkling) was firstly converted into the bit stream, which was then encoded onto the BASK microwave signal through the microwave transmitter to drive and modulate the metasurface converter for generating the green OOK laser signal. The generated OOK laser signal across underwater was then received by the photoelectric detection and demodulation circuit and further demodulated into the digital baseband signal via the laser receiver to recover the video. For water-to-air wireless communication, the video (lotus blooming) was firstly converted into the bit stream, which was then encoded onto the underwater green OOK laser signal through the laser transmitter to modulate the metasurface converter; after that, the reflection amplitude response of the metasurface was rapidly altered to directly

convert the OOK laser signal to the air BASK microwave signal. The reflected BASK microwave signal was then received by the horn antenna and demodulated into the digital baseband signal via the SDR platform to recover the video. See “Methods” for detailed workflow of the system prototype. The entire transmission process is presented in Supplementary Movie 1 and is described briefly in Supplementary Note 6. Data rates of 400 and 100 kbps over the microwave-to-underwater-laser and underwater-laser-to-microwave transmission links can be achieved, respectively. The results validate that two different videos are transmitted independently and simultaneously cross bidirectional air-water interfaces by the metasurface-enabled full-duplex laser-microwave hybrid wireless communication system.

We demonstrated that two small laser beams can illuminate both photodiodes simultaneously to modulate the microwave reflections of metasurface. Therefore, on the metasurface, spatial diversity transmission^{47,48} can be developed and used to reduce the turbulence-induced underwater optical signal fluctuation. We further experimentally investigate the transmission performance of the metasurface-enabled laser-to-microwave wireless link when underwater turbulence is induced. The experimental setup is shown in Fig. 4a. To generate obvious temperature-induced underwater turbulence, 20° tap water was first injected into the water tank, and then 60° hot water was injected into it from the top to bottom. In experiments, we tested the video transmission quality of the laser-to-microwave link when metasurface is illuminated by one laser signal and two identical laser signals simultaneously, and the transmission results are shown in Fig. 4b, c, respectively. For the case that one photodiode is illuminated, strong turbulence will cause the laser beam diffusion and drift in a short period of time, thereby reducing the transmission quality of the link. However, when two photodiodes are illuminated simultaneously, the link can still provide relatively stable data transmission, because even though one laser beam is in outage, the other still ensures reliable

operation, thus mitigating the impact of underwater turbulence. See Supplementary Movie 2 for entire transmission process.

Discussion

Transmission rates of the bidirectional links mainly depend on the switching speed of the loaded diodes and the used signal modulation mode (see Supplementary Note 7 for more discussions). Therefore, the following potential improvements could be adopted in future to increase the link rate. Firstly, in the current scheme, to achieve minimal energy consumption, there is no voltage source to connect to metasurface. External bias can be used to reduce the charge and discharge time of carriers, thereby increasing the switching speed of diodes. Secondly, in the future, we will have more opportunities to choose diodes with faster switching speeds. Finally, developing high-order modulation schemes such as quadrature amplitude modulation on the metasurface can help improve the link rates. It should be noted that by selecting the Schottky diode and photodiode with high cut-off frequencies, we are able to extend the metasurface to higher microwave frequencies for achieving greater channel bandwidth. For example, we have designed a metasurface operating at above 12 GHz, as discussed in Supplementary Note 8. Our metasurface does not need to be connected to any external power supplies, which is highly desired in marine environments. To further demonstrate the application potential of the metasurface-enabled air-water cross-media wireless links for satellite-ground-ocean integrated network, we have provided more results and discussion (Supplementary Note 9) on air satellite communication and underwater long-distance communication.

In summary, we have demonstrated a programmable metasurface capable of direct free-space microwave-to-laser and reverse conversions for full-duplex cross-media wireless communications. The metasurface converter was realized by integrating the Schottky diodes and photodiodes into the double-sided subwavelength resonant structures simultaneously. With this heterogeneous design, the metasurface combines multi-physical control, information modulation, and signal conversion functionalities into a shared-aperture platform, showing great promise as the basis of wave-matter-information interaction interfaces. The results validate that the real-time bidirectional conversion between microwave and laser signals can be well achieved, without multiple separated devices and complex processes, which is critical for the development of full-duplex and low-overhead cross-media transmission system. We developed a full-duplex air-water cross-media wireless communication architecture based on this metasurface and constructed a system prototype by further designing the microwave and laser transceivers. The tank experiments show that two different videos can be transferred from the air-to-underwater and underwater-to-air channels simultaneously and independently through the microwave-to-laser and laser-to-microwave links, respectively. Our work opens new horizons for bidirectional, zero-power, cost-effective conversion interfaces that are fundamentally important to fully-connected 6G communication, and also hint at a far richer physics that paves the way for new interaction regimes between electronics and photonics in the wave domain.

Methods

Meta-element design

The integrated Schottky diode and photodiode are critical components for the meta-element, and they operate at DC-supply-free state. Unlike other diodes, Schottky diode contains an MS junction with low forward voltage drop and fast switching speed, which is very suitable for rectification. The loaded inductor is used to connect adjacent meta-elements to reduce EM coupling, and to filter the alternating-current component in the output voltage. The photodiode is controlled completely by laser. Based on polarization multiplexing, under *x*-polarized microwave incidence, Resonant Structure 1 operates and Resonant Structure 2 acts as a metal ground to ensure strong

microwave absorption; under *y*-polarized microwave incidence, Resonant Structure 2 operates to realize the microwave reflection. Since the metal proportion of Resonant Structure 1 is very small, EM waves can go through from the front of the meta-element and interact with Resonant Structure 2. The middle layer is a 2.0-mm-thickness dielectric with a permittivity $\varepsilon = 2.65$ and a loss tangent $\tan \delta = 0.001$. The side length of the meta-element is 15.0 mm, which is $0.2\lambda_0$ at 4.00 GHz. The other structure parameters (Supplementary Fig. 2) are optimized to achieve the high absorptivity and large reflection amplitude difference.

Array design and metasurface fabrication

For microwave-to-laser up-conversion metasurface, along the *x* direction, 20 Resonant Structures 1 in one row are connected naturally in series. Along the *y* direction, 10 same rows are connected in parallel by two metal wires on both sides, which are further connected to two feeding lines through two metallic vias. These two feeding lines are connected to the positive and negative electrodes of the integrated laser diode, respectively. For laser-to-microwave down-conversion metasurface, along the *x* direction, these 20 Resonant Structures 2 in one row are connected naturally in parallel by their patches. Along the *y* direction, two patches in every row are connected to two of the designed metal lines at both sides of the metasurface sample through stubs, as shown in Supplementary Fig. 7. Under this connection relationship, all the photodiodes are connected in parallel. The metasurface sample was fabricated by the low-cost printed circuit board technology, and Schottky diodes, photodiodes, chip inductors, a chip resistor, and a laser diode were welded precisely on the metasurface by the well-developed machine welding procedure. The metasurface covers an effective area of $300 \times 150 \text{ mm}^2$.

Experiments on microwave-laser conversion

The experimental setups of the microwave-laser bidirectional conversion are shown in Supplementary Fig. 8. In the experiment of microwave to laser (Supplementary Fig. 8a), we increased continuously the incident microwave power to record the emission power of the laser diode by a laser power meter. The microwave was output by a microwave generator (NI PXIe-564) and then amplified by a power amplifier. The amplified microwave was emitted by a horn antenna to shine the metasurface sample. The horn antenna with gain of 15 dBi was fixed 0.1 m away from the metasurface sample, and thus the microwave transmission efficiency is 99.9% (see Supplementary Note 4 for more details). In this case, the microwave power radiated by the horn antenna is almost completely received by the metasurface. Thus, when the input microwave power reaches enough intensity of 25 mW, the corresponding illuminated power density is about 0.056 mW/cm^2 . The microwave-to-laser conversion efficiency is defined as the ratio of the output laser power to the microwave power received by metasurface. In the experiment of laser to microwave (Supplementary Fig. 8b), the horn antenna was connected to a vector network analyzer for emitting microwave and then receiving the reflection energy from the metasurface sample. The laser source was adopted to emit green lasers for controlling the sample. The diameter of the laser spot was about 4.0 mm.

Details on system prototype

The built full-duplex microwave-laser hybrid wireless communication system across air-water media mainly includes three parts: a microwave transceiver, a metasurface converter, and a laser transceiver. The microwave transmitter consists of a software-defined radio (SDR) platform (NI USRP-2954), a power amplifier, and a *x*-polarized horn antenna to emit the amplified BASK signal. In microwave receiver, the feeding antenna connected to a microwave generator was adopted to provide incident *y*-polarized monochromatic microwave, and then the reflected BASK microwave signal was received by the *y*-polarized horn

antenna to transmit the signal to the SDR connected to a post-processing computer. The laser transmitter contains a field programmable gate array (FPGA) and a green laser diode, which was designed to generate the OOK laser signal with the modulated information. The laser receiver contains a high-speed and high-sensitivity photoelectric detection and demodulation circuit (Supplementary Note 5) and a connected post-processing computer. In the experiment, the distance from the laser diode to the metasurface sample was about 1.3 m. The incident *x*- and *y*-polarized microwave frequencies are 4.06 and 4.45 GHz, respectively. To reduce the required microwave signal power, the *x*-polarized horn antenna was placed closely to the metasurface sample for achieving high transmission efficiency. The gain of the used *y*-polarized horn antenna is 11 dBi at 4.45 GHz, and it was fixed 0.25 m away from the metasurface sample. By using Eq. (S2), the far-field transmission efficiency is calculated as about 74.5%.

Workflow of the system

The detailed workflow of the full-duplex air–water cross-media wireless communication system is illustrated in Supplementary Fig. 12. For microwave-to-laser transmission link, the star twinkling (Tx Video 1) is firstly converted into the bit stream and is used to modulate the SDR platform to generate the corresponding BASK microwave signal. Then, the generated BASK microwave signal is amplified by the connected power amplifier to provide the required signal power. When receiving the amplified BASK microwave signal, the metasurface platform will generate the corresponding OOK green laser signal through the integrated laser diode. The generated OOK laser signal will be transmitted in the underwater channel and is finally captured by the photoelectric detection and demodulation circuit connected to a post-processing computer for recovering the original video. For laser-to-microwave transmission link, the lotus blooming (Tx Video 2) is firstly converted into the bit stream, which controls the FPGA to generate the corresponding voltages to modulate the laser diode for generating the OOK laser signal. When receiving the OOK laser signal transmitted from the underwater channel, the metasurface platform will generate the BASK microwave signal under the monochromatic wave incidence. Finally, the reflected BASK microwave signal is received by a horn antenna and is further demodulated into the digital baseband signal via the SDR platform to recover the original video.

Data availability

The data that support the findings of this study are available within the manuscript and its Supplementary Information. Source data are provided with this paper.

References

- Bloch, J., Cavalleri, A., Galitski, V., Hafezi, M. & Rubio, A. Strongly correlated electron-photon systems. *Nature* **606**, 41–48 (2022).
- Marpaung, D., Yao, J. & Capmany, J. Integrated microwave photonics. *Nat. Photon.* **13**, 80–90 (2019).
- Sahu, R. et al. Entangling microwaves with light. *Science* **380**, 718–721 (2023).
- Salamin, Y. et al. Microwave plasmonic mixer in a transparent fibre-wireless link. *Nat. Photon.* **12**, 749–753 (2018).
- Zhang, X. G. et al. A metasurface-based light-to-microwave transmitter for hybrid wireless communications. *Light. Sci. Appl.* **11**, 126 (2022).
- Ummethala, S. et al. THz-to-optical conversion in wireless communications using an ultra-broadband plasmonic modulator. *Nat. Photon.* **13**, 519–524 (2019).
- Montanaro, A. et al. Sub-THz wireless transmission based on graphene-integrated optoelectronic mixer. *Nat. Commun.* **14**, 6471 (2023).
- Chowdhury, M. Z. et al. Optical wireless hybrid networks: trends, opportunities, challenges, and research directions. *IEEE Commun. Surv. Tutor.* **22**, 930–966 (2020).
- Ma, Y., Zhang, Q. & Wang, H. 6G: ubiquitously extending to the vast underwater world of the oceans. *Engineering* **8**, 12–17 (2022).
- Luo, H. et al. Recent progress of air/water cross-boundary communications for underwater sensor networks: a review. *IEEE Sens. J.* **22**, 8360–8382 (2022).
- Ayata, M. et al. High-speed plasmonic modulator in a single metal layer. *Science* **358**, 630–632 (2017).
- Salamin, Y. et al. Direct conversion of free space millimeter waves to optical domain by plasmonic modulator antenna. *Nano Lett.* **15**, 8342–8346 (2015).
- Koch, U. et al. A monolithic bipolar CMOS electronic-plasmonic high-speed transmitter. *Nat. Electron.* **3**, 338–345 (2020).
- Kuznetsov, A. S., Biermann, K., Reynoso, A. A., Fainstein, A. & Santos, P. V. Microcavity phononitons—a coherent optical-to-microwave interface. *Nat. Commun.* **14**, 5470 (2023).
- Bochmann, J., Vainsencher, A., Awschalom, D. D. & Cleland, A. C. Nanomechanical coupling between microwave and optical photons. *Nat. Phys.* **9**, 712–716 (2013).
- Borówka, S., Pylypenko, U., Mazelanik, M. & Parniak, M. Continuous wideband microwave-to-optical converter based on room-temperature Rydberg atoms. *Nat. Photon.* **18**, 32–38 (2024).
- Stockill, R. et al. Ultra-low-noise microwave to optics conversion in gallium phosphide. *Nat. Commun.* **13**, 6583 (2022).
- Zhang, X. G. et al. Optoelectronic metasurface for free-space optical-microwave interactions. *ACS Appl. Mater. Interfaces* **15**, 22744–22751 (2023).
- Yu, N. et al. Light propagation with phase discontinuities: generalized laws of reflection and refraction. *Science* **334**, 333–337 (2011).
- Luo, X. Principles of electromagnetic waves in metasurfaces. *Sci. China Phys. Mech. Astron.* **58**, 594201 (2015).
- Sun, S., He, Q., Hao, J., Xiao, S. & Zhou, L. Electromagnetic metasurfaces: physics and applications. *Adv. Opt. Photonics* **11**, 380–479 (2019).
- Cui, T. J., Qi, M. Q., Wan, X., Zhao, J. & Cheng, Q. Coding metamaterials, digital metamaterials and programmable metamaterials. *Light Sci. Appl.* **3**, e218 (2014).
- Cui, T. J. et al. Information metamaterial systems. *iScience* **23**, 101403 (2020).
- Tian, H. W. et al. Programmable controlling of multiple spatial harmonics via a nonlinearly phased grating metasurface. *Adv. Funct. Mater.* **32**, 2203120 (2022).
- Zhang, X. G. et al. Polarization-controlled dual-programmable metasurfaces. *Adv. Sci.* **7**, 1903382 (2020).
- Chen, M. K. et al. A meta-device for intelligent depth perception. *Adv. Mater.* **34**, 2107465 (2022).
- Benea-Chelms, I.-C. et al. Gigahertz free-space electro-optic modulators based on Mie resonances. *Nat. Commun.* **13**, 3170 (2022).
- Ren, H. R. et al. Complex-amplitude metasurface-based orbital angular momentum holography in momentum space. *Nano-technol.* **15**, 948–955 (2020).
- Wang, X. et al. Metasurface-based realization of photonic time crystals. *Sci. Adv.* **9**, eadg7541 (2023).
- Wu, G.-B. et al. A universal metasurface antenna to manipulate all fundamental characteristics of electromagnetic waves. *Nat. Commun.* **14**, 5155 (2023).
- Zhang, X. G. et al. Smart Doppler cloak operating in broad band and full polarizations. *Adv. Mater.* **33**, 2007966 (2021).
- Shaltout, A. M., Shalaev, V. M. & Brongersma, M. L. Spatiotemporal light control with active metasurfaces. *Science* **364**, eaat3100 (2019).

33. Engheta, N. Metamaterials with high degrees of freedom: space, time, and more. *Nanophotonics* **10**, 639–642 (2021).
34. Mikhcheeva, E. et al. Space and time modulations of light with meta-surfaces: recent progress and future prospects. *ACS Photonics* **9**, 1458–1482 (2022).
35. Shadrivov, I. V., Kapitanova, P. V., Maslovski, S. I. & Kivshar, Y. S. Metamaterials controlled with light. *Phys. Rev. Lett.* **109**, 083902 (2012).
36. Zhang, X. G. et al. An optically driven digital metasurface for programming electromagnetic functions. *Nat. Electron.* **3**, 165–171 (2020).
37. Zhang, X. G. et al. Light-controllable time-domain digital coding metasurfaces. *Adv. Photonics* **4**, 025001 (2022).
38. Agheli, P., Beyranvand, H. & Emadi, M. J. UAV-assisted underwater sensor networks using RF and optical wireless links. *J. Light Technol.* **39**, 7070–7082 (2021).
39. Li, S., Yang, L., Costa, D. B. D., Renzo, M. D. & Alouini, M.-S. On the performance of RIS-assisted dual-hop mixed RF-UWOC systems. *IEEE Trans. Cogn. Commun. Netw.* **7**, 340–353 (2021).
40. Islam, M. S., Younis, M., Mahmud, M., Carter, G. & Choa, F.-S. A peak detection based OOK photoacoustic modulation scheme for air to underwater communication. *Opt. Commun.* **529**, 129078 (2023).
41. Li, Y., Wang, S., Jin, C., Zhang, Y. & Jiang, T. A survey of underwater magnetic induction communications: fundamental issues, recent advances, and challenges. *IEEE Commun. Surv. Tutor.* **21**, 2466–2487 (2019).
42. Qu, F. et al. Cross-medium communication combining acoustic wave and millimeter wave: theoretical channel model and experiments. *IEEE J. Ocean. Eng.* **47**, 483–492 (2022).
43. Shi, Q., He, Z., Xu, H., Gao, J. & Zhao, P. Research on information transmission technology through the water-air interface combining a sonar and a radar. *IEEE Sens. J.* **23**, 7616–7625 (2023).
44. Afzal, S. S. et al. Battery-free wireless imaging of underwater environments. *Nat. Commun.* **13**, 5546 (2022).
45. Phon, R. & Lim, S. Dynamically self-reconfigurable multifunctional all-passive metasurface. *ACS Appl. Mater. Interfaces* **12**, 42393–42402 (2020).
46. Erkmen, F., Almoneef, T. S. & Ramahi, O. M. Electromagnetic energy harvesting using full-wave rectification. *IEEE Trans. Microw. Theory Tech.* **65**, 1843–1851 (2017).
47. Vali, Z., Gholami, A., Ghassemloooy, Z., Omoomi, M. & Michelso, D. G. Experimental study of the turbulence effect on underwater optical wireless communications. *Appl. Opt.* **57**, 8314–8319 (2018).
48. Liu, W., Jiang, W., Huang, N. & Xu, Z. Experimental investigation of underwater optical wireless communication for correlated SIMO channel under temperature-induced turbulence. *IEEE Photon. J.* **15**, 7302907 (2023).

Acknowledgements

This work was supported by the National Natural Science Foundation of China under Grants 62201143 (X.G.Z.), 62288101 (T.J.C.), and U23B2015 (W.X.J.), the Natural Science Foundation of Jiangsu Province under Grants BK20220807 (X.G.Z.) and BK20212002 (T.J.C.), the China National Postdoctoral Program for Innovative Talents under Grant BX2021063 (X.G.Z.), the China Postdoctoral Science Foundation under Grant 2021M700762 (X.G.Z.), the Postgraduate Research & Practice

Innovation Program of Jiangsu Province under Grant KYCX23_0251 (Y.L.S.), the Fundamental Research Funds for the Central Universities under Grant 2242023K5002 (W.X.J.), and the 111 Project under Grant 111-2-05 (T.J.C.).

Author contributions

X.G.Z., W.X.J., C.-W.Q., T.J.C., and Z.Z. conceived the research idea. X.G.Z. designed the scheme, and performed the simulations and experiments in coordination with Y.L.S. and B.Z. X.G.Z. carried out the theoretical analysis and developed the metasurface. Y.L.S., X.G.Z., and B.Z. designed and built the laser and microwave transceivers. X.G.Z. and Y.L.S. conducted the system measurements with the help of H.W.T. and B.Y.W. X.G.Z. and Y.L.S. collected and analyzed the data with contributions from all co-authors. X.G.Z., W.X.J., C.-W.Q., and T.J.C. co-wrote the manuscript with input and comments from all the authors. W.X.J., C.-W.Q., T.J.C., and Z.Z. supervised and coordinated the project.

Competing interests

The authors declare no competing interests.

Additional information

Supplementary information The online version contains supplementary material available at <https://doi.org/10.1038/s41467-025-55940-9>.

Correspondence and requests for materials should be addressed to Zaichen Zhang, Cheng-Wei Qiu, Tie Jun Cui or Wei Xiang Jiang.

Peer review information *Nature Communications* thanks Yannick Salamin, and the other, anonymous, reviewer(s) for their contribution to the peer review of this work. A peer review file is available.

Reprints and permissions information is available at <http://www.nature.com/reprints>

Publisher's note Springer Nature remains neutral with regard to jurisdictional claims in published maps and institutional affiliations.

Open Access This article is licensed under a Creative Commons Attribution-NonCommercial-NoDerivatives 4.0 International License, which permits any non-commercial use, sharing, distribution and reproduction in any medium or format, as long as you give appropriate credit to the original author(s) and the source, provide a link to the Creative Commons licence, and indicate if you modified the licensed material. You do not have permission under this licence to share adapted material derived from this article or parts of it. The images or other third party material in this article are included in the article's Creative Commons licence, unless indicated otherwise in a credit line to the material. If material is not included in the article's Creative Commons licence and your intended use is not permitted by statutory regulation or exceeds the permitted use, you will need to obtain permission directly from the copyright holder. To view a copy of this licence, visit <http://creativecommons.org/licenses/by-nc-nd/4.0/>.

© The Author(s) 2025